

# An architectural approach to the oxygen permeability of a $\text{La}_{0.6}\text{Sr}_{0.4}\text{Fe}_{0.9}\text{Ga}_{0.1}\text{O}_{3-\delta}$ perovskite membrane

Grégory Etchegoyen<sup>a</sup>, Thierry Chartier<sup>a,\*</sup>, Pascal Del-Gallo<sup>b</sup>

<sup>a</sup> *Laboratoire de Science des Procédés Céramiques et Traitements de Surface (SPCTS), UMR-CNRS 6638, ENSCI, 47-73 Av. Albert Thomas, 87065 Limoges, France*

<sup>b</sup> *AIR LIQUIDE, Centre de Recherche Claude-Delorme, 1 chemin de la Porte des Loges, BP. 126, 78354 Jouy-en-Josas, France*

Received 10 April 2005; received in revised form 26 May 2005; accepted 4 June 2005

Available online 8 August 2005

## Abstract

Multilayer membranes based on  $\text{La}_{0.6}\text{Sr}_{0.4}\text{Fe}_{0.9}\text{Ga}_{0.1}\text{O}_{3-\delta}$  (LSFG) and  $\text{La}_{0.6}\text{Sr}_{0.4}\text{Co}_{0.8}\text{Fe}_{0.2}\text{O}_{3-\delta}$  (LSCF) perovskite materials were fabricated to study the impact of membrane architecture on the oxygen permeability. Thick dense membrane and asymmetric membranes were shaped by tape casting and stacked to reach the desired architecture. Asymmetric membranes composed of a thin dense LSFG layer (120  $\mu\text{m}$ ) and a thick porous support layer (820  $\mu\text{m}$ ) of the same material were co-sintered to obtain crack-free and flat membranes. The use of large corn-starch particles (14  $\mu\text{m}$ ) as pore forming agent to the tape-casting slurries resulted in a connected porosity in the sintered support layer with low gas diffusion resistance. Oxygen permeation measurements in an air/argon gradient between 800 and 925 °C showed that the thickness of self-supported LSFG membranes was not the determining factor in the membrane performance for our testing conditions. A catalytic layer of  $\text{La}_{0.6}\text{Sr}_{0.4}\text{Co}_{0.8}\text{Fe}_{0.2}\text{O}_{3-\delta}$  (LSCF), deposited on the membrane surfaces to catalyze the oxygen exchange reactions, leads to a significant increase of oxygen permeation rates. As the membrane thickness had no effect even if a catalyst coating was used, surface-exchange reactions were thought to be still limiting for the oxygen permeation fluxes. Thus, the improvement of surface activity of LSFG membrane was found to be a key point to reach higher oxygen permeation fluxes.

© 2005 Elsevier Ltd. All rights reserved.

**Keywords:** Membrane; Perovskites; Permeability;  $(\text{La},\text{Sr})(\text{Fe},\text{Ga})\text{O}_3$

## 1. Introduction

Catalytic membrane reactors (CMR) for partial oxidation of methane are subjected to an increasing interest since they were found to allow conversion of natural gas to synthesis gas, i.e. an  $\text{H}_2$  and CO mixture, with a better efficiency and a lower cost than conventional processes.<sup>1–4</sup> These reactors make it possible to achieve, in a single step, the separation of oxygen from air on one side of the membrane and the catalytic partial oxidation of methane to syngas on the other face at about 750 °C.<sup>5–10</sup>

To operate without the need of an external electronic circuit, the membrane material has to exhibit both ionic

and electronic conductivity. Ceramic membranes based on perovskite-type oxides ( $\text{ABO}_3$ ), suitably doped on the A and/or B site, may exhibit ionic and electronic conductivities at temperature typically higher than 700 °C.<sup>11–16</sup> When such dense perovskite membranes are exposed to an oxygen partial pressure gradient between their opposite faces, an anionic oxygen flux takes place through the membrane bulk from the oxygen-rich side to the oxygen-lean side.

During the last decades, an important research effort has been focused on materials able to provide high oxygen permeation rates and long term stability in the process conditions.  $\text{La}_{1-x}\text{Sr}_x\text{Fe}_{1-y}\text{Ga}_y\text{O}_3$  perovskites were found to be promising materials because of their good chemical stability under a reducing environment, their high oxygen-ionic conductivity and their low dimensional variation when submitted to oxygen gradients.<sup>17–22</sup>

\* Corresponding author. Tel.: +33 5 5545 2222; fax: +33 5 5579 0998.  
E-mail address: [t.chartier@ensci.fr](mailto:t.chartier@ensci.fr) (T. Chartier).

Nevertheless, self-supported thick dense membranes cannot reach the oxygen flux requirement of  $10 \text{ ml cm}^{-2} \text{ min}^{-1}$  to make CMR technology competitive with the traditional syngas production route, i.e. steam methane reforming (SMR) and auto thermal reforming (ATR).<sup>23</sup> Indeed, the oxygen transport includes different resistive steps, such as oxygen exchange on the surfaces of the membrane or oxygen ionic diffusion in the membrane bulk, which result in losses in the overall oxygen permeation kinetics. So, the oxygen flux can be significantly improved by acting on the limiting step, for example by decreasing the dense membrane thickness when the bulk diffusion is dominating,<sup>24–28</sup> or by coating the membrane with a catalyst to enhance oxygen surface exchanges.<sup>29–32</sup>

The purpose of this study is to examine the potential of the composition  $\text{La}_{0.6}\text{Sr}_{0.4}\text{Fe}_{0.9}\text{Ga}_{0.1}\text{O}_{3-\delta}$  (referenced as LSFG) as mixed-conducting material for CMR application and to study the impact of membrane architecture on oxygen permeation flux.

The effect of dense membrane thickness on oxygen permeation rate was evaluated with self-supported membranes for a thickness ranging from 1.30 to 0.63 mm. For thinner membranes (<0.6 mm) a separate porous support is needed to ensure the mechanical integrity of the membrane. This support has to allow gas species diffusion up to the dense layer. In these asymmetric membranes, the same material (LSFG) was used for the dense and porous layers as previously proposed by Jin et al.;<sup>26</sup> thus the chemical and thermal compatibility between the layers is guaranteed. In addition, the mixed-conducting properties of the porous layer can improve the oxygen flux by shifting the oxygen exchanges at gas/solid interfaces to the inside of the whole porous layer thickness.

To identify the oxygen permeation regime, a catalytic layer was coated on one or both sides of several membranes. This layer makes it possible to increase the oxygen surface-exchange coefficient thanks to its catalytic activity for oxygen reduction and re-oxidation and by developing active surface area (microporous layer). Perovskite of the general formula  $\text{La}_{1-x}\text{Sr}_x\text{Co}_{1-y}\text{Fe}_y\text{O}_{3-\delta}$  often used as a cathode material for the solid oxide fuel cell (SOFC)<sup>33</sup> due to its high electronic and ionic conductivities and its excellent catalytic activity<sup>12–14</sup> was chosen as a catalytic material.

## 2. Experimental

### 2.1. Powders synthesis

The LSFG powder was synthesized through a solid-state reaction as described previously.<sup>34</sup> Appropriate amounts of  $\text{La}_2\text{O}_3$ ,  $\text{Fe}_2\text{O}_3$ ,  $\text{Ga}_2\text{O}_3$  and  $\text{SrCO}_3$  were weighed, and briefly milled in a mortar. The mixture was then finely attrition-milled using zirconia media in ethanol for 3 h, separated the charge, dried and calcined at  $1100^\circ\text{C}$  for 10 h.

The synthesized powder was then attrition-milled using zirconia balls and ethanol in order to decrease the average

grain size down to  $0.8 \mu\text{m}$  which was directly controlled on a sample of suspension with a laser granulometer (Mastersizer 2000, Malvern Instruments).

The LSCF powder was synthesized starting from  $\text{La}_2\text{O}_3$ ,  $\text{SrCO}_3$ ,  $\text{Fe}_2\text{O}_3$  and  $\text{Co}_2\text{O}_3$  powders with the same protocol as used for LSFG.

### 2.2. Dense membrane preparation

The various configurations of prepared membranes are presented in Fig. 1.

An amount of 5 vol% of magnesia (grain size =  $0.5 \mu\text{m}$ ) was added to the LSFG powder to control the sintered membrane microstructure as explained in a previous paper.<sup>34</sup>

The LSFG/MgO powder was planetary milled for 5 h in the azeotropic mixture of butanone-2 and ethanol, with a dispersant (phosphate ester). Then, an acrylic binder (methyl methacrylate, Degalan LP51/07, Degussa) and a phthalate plasticizer (dibutyl phthalate, Sigma–Aldrich,) were added to the slurry with a subsequent 10-h ball-milling. The tape-casting formulation is given in Table 1. After de-airing for 2 days at a very slow rotation speed and verifying the viscosity, the slurry was tape-cast on a polymeric film using a doctor blade device to obtain green tapes with a thickness of  $150 \mu\text{m}$ . Then, 30 mm-diameter disks were punched from the green tapes, stacked and laminated under a pressure of 50 MPa at a temperature of  $70^\circ\text{C}$  to obtain defect-free green membranes.

These green membranes were slowly debinded at  $550^\circ\text{C}$  in air and sintered at  $1300^\circ\text{C}$  for 2 h in a 90% nitrogen/10% oxygen atmosphere.

### 2.3. Asymmetric membrane preparation

Porous LSFG membranes were obtained by adding to the previous slurries, a fugitive material that will burn out, leaving large connected pores in the membrane. Fourteen micrometers mean diameter corn-starch particles were used as fugitive agent because of their spherical shape, their narrow size distribution and their total combustion during thermal treatment.

Corn-starch particles were added to the slurry after the 10-h ball-milling stage to obtain a 40 vol% corn-starch, 60 vol%

Table 1  
Slurry composition for tape-casting

	Volume (%)
Powders	
LSFG	24.4
MgO	1.3
Dispersant (phosphate ester)	2.0
Solvent	
Ethanol	19.5
Butanone-2	37.7
Binder (methyl methacrylate)	8.4
Plasticizer (dibutyl phthalate)	6.7



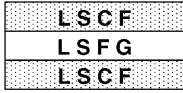


Description	Abbreviation	
LSFG dense membrane	LSFG	$pO_2'$  $pO_2'$ $pO_2' > pO_2''$
LSFG dense membrane coated with LSCF on permeate side	psc-LSFG	
LSFG dense membrane coated with LSCF on feed and permeate sides	fpsc-LSFG	
LSFG asymmetric membrane	LSFG-am	
LSFG asymmetric membrane coated with LSCF on dense layer (feed side)	fsc-LSFG-am	

Fig. 1. Architectural description and abbreviation of prepared membrane.

mineral powder slurry. After a subsequent homogenization and de-airing phase, the slurry was tape-cast to obtain a 150- $\mu\text{m}$  thick tape from which 30 mm-diameter disks were punched. Asymmetric membranes were elaborated by stacking seven disks of a corn starch containing tape (porous layer) and 1 disk of a tape without pore forming agent (dense layer).

Asymmetric membranes were slowly debinded and sintered with the same thermal cycle as dense membranes.

#### 2.4. Catalyst coating

A 20- $\mu\text{m}$  thick porous layer of  $\text{La}_{0.6}\text{Sr}_{0.4}\text{Co}_{0.8}\text{Fe}_{0.2}\text{O}_{3-\delta}$  (referenced as LSCF) was deposited on membrane surfaces using screen-printing. The screen-printing slurry was a mixture of 35 vol% of LSCF powder, 63 vol% of resin (3% of ethylcellulose dissolved in terpineol) and 2 vol% of a dispersant. After homogenization using a three-cylinder system, the slurry was deposited on sintered disks through a 44  $\mu\text{m}$  sieve. Dense membranes were screen-printed on one or both sides, while asymmetric membranes were only screen-printed on the dense layer side.

The coated membranes were dried at room temperature and fired at 1000 °C for 1 h in a 10%  $\text{O}_2$ /90%  $\text{N}_2$  controlled atmosphere.

#### 2.5. Characterization

Phase crystallographic structures were determined by X-ray diffraction (XRD) using Cu  $\text{K}\alpha 1$  radiation.

Gas permeability of the sintered supports was measured on a 1.2-mm thick porous support using argon at room temperature. Porous supports were submitted to an argon pressure flow from 0.105 to 0.175 MPa on one face while the opposite

face remains at atmospheric pressure. Outlet gas flows were measured using a soap bubble flowmeter.

Membrane microstructures and architectures were observed using a scanning electron microscope (S-2500, Hitachi) on fractured or polished cross sections.

#### 2.6. Oxygen permeation measurement

Oxygen permeation fluxes were measured on a specific device (Fig. 2), composed of a tubular furnace, gas feeders and gas analyzers (gas chromatograph and YSZ-based oxygen sensor). Membranes were sealed on the top of an alumina tube and inserted in the vertical furnace at room temperature.

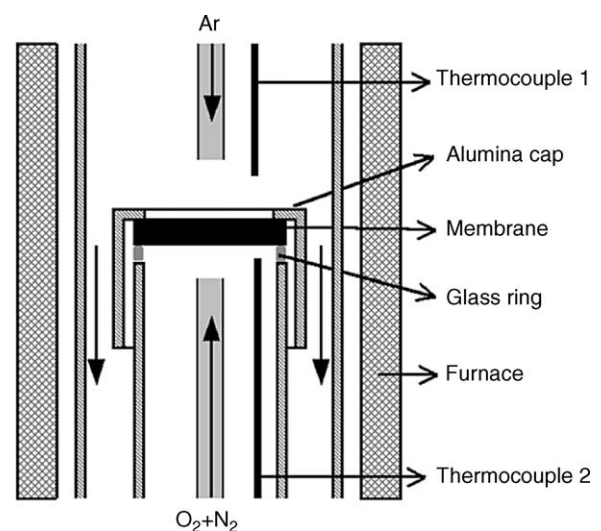


Fig. 2. Schematic view of the membrane testing system.

The inner compartment ( $O_2 + N_2$ ) and the outside compartment (Ar) were made gas-leak proof thanks to a Pyrex-based glass ring placed between the membrane and the alumina support tube as suggested by Qi.<sup>36</sup> An alumina cap was placed on the top of the membrane in order to apply a pressure on the glass sealing ring. The furnace was heating up in air at a temperature above the glass softening temperature of the sealing ring. After sealing, the membrane was submitted to an argon flow on its upper face and to a recombined air flow (79%  $N_2 + 21\%$   $O_2$ ) on its bottom face, both flow rates were  $200 \text{ ml (STP) min}^{-1}$ . Membrane and seal tightness were verified by controlling the nitrogen level in the outlet product gases with the chromatograph (CP 3380, Varian). Permeation measurements were performed in a temperature range from 800 to 925 °C. The temperatures given are the average of the values measured with thermocouple 1 and 2 (Fig. 2). Oxygen permeation fluxes are calculated from the experimental data from the relation:

$$j_{O_2} = \frac{CF}{S} \alpha \quad (1)$$

where  $j_{O_2}$  is the oxygen permeation flux ( $\text{ml cm}^{-2} \text{ min}^{-1}$ );  $C$ , the permeating oxygen concentration in the argon flow (ppm);  $F$ , the argon flow rate ( $\text{ml min}^{-1}$ );  $S$ , the membrane effective surface area ( $\text{cm}^2$ ) and  $\alpha$  a coefficient of normalization for standard temperature and pressure.

### 3. Results and discussion

#### 3.1. XRD characterization

The crystallographic phase of the synthesized LSF and LSCF powders and of a crushed LSF asymmetric membrane were verified by XRD (Fig. 3). A perovskite structure was found for all the samples. The crushed membrane pattern

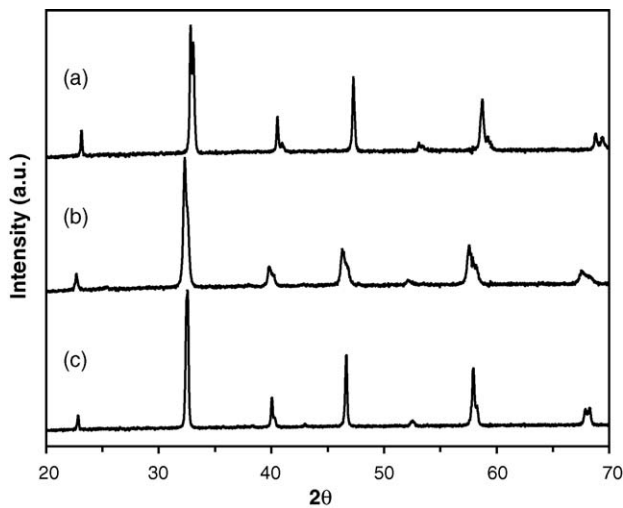


Fig. 3. XRD patterns of synthesized powders and of a crushed LSF membrane: (a) LSCF powder; (b) LSF powder; (c) LSF asymmetric membrane.

reveals the presence of a single perovskite phase which is the same for the dense layer and the porous one. Changes in XRD patterns of LSF powder and asymmetric membrane can be only attributed to an increase of the crystallite size during sintering that reduces peak width, and to the presence of MgO inclusions in the membrane that explains an additional small peak near 43°.

#### 3.2. Porous support

Pore size and porous volume of the porous support have to satisfy the requirements in terms of mechanical integrity and gas permeability. The connected porosity of the sintered supports was determined to be about 30% by Archimedes method. As the starting slurries contained 40% pore forming agent per mineral part, about 10% of porosity was lost during the sintering stage. Micrographs of the fractured section of a porous membrane show large connected pores with a size ranging from 8 to 20  $\mu\text{m}$ , that corresponds to the size of the corn-starch particles introduced in the slurry (Fig. 4). The bulk that surrounds the pores is dense with a small grain size of about 1  $\mu\text{m}$ . Pore size and pore volume would likely ensure easy gas diffusion through open porosity but the narrow pore interconnections could be resistive to the gas flow.

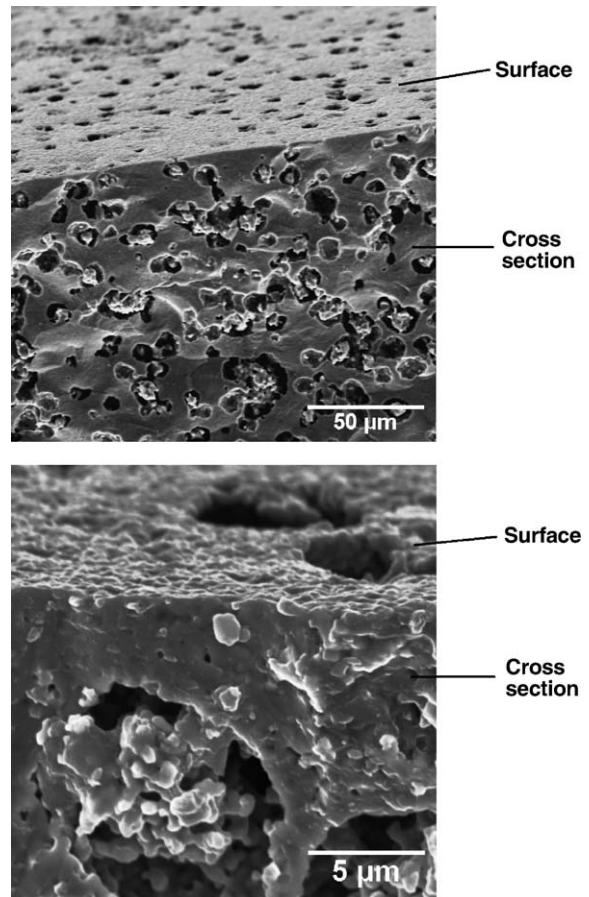


Fig. 4. SEM micrographs of the porous LSF support; perspective views at two magnifications.



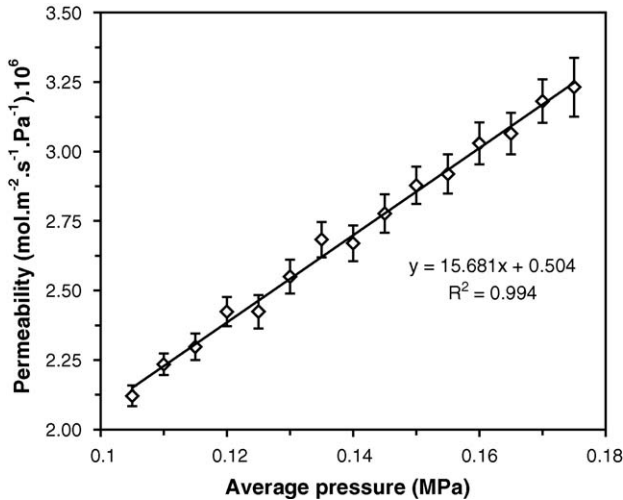


Fig. 5. Argon permeability of a 1.2 mm thick porous membrane at room temperature.

Fig. 5 shows the evolution of argon permeability as a function of the mean pressure for a 1.2-mm thick porous membrane. The linear pressure dependence of the permeability suggests that the viscous flow regime (Poiseuille flow) is dominating in front of Knudsen diffusion and further that the diameter of the pore interconnections are larger than the mean free path of the gas molecules (about 300 nm at 300 K and 1 atm). The average radius of the pore interconnections can be calculated with the following relation<sup>35</sup> using the equation of the fitted line in Fig. 5:

$$r = \frac{16S\eta}{3K} \sqrt{\frac{8RT}{\pi M}} \quad (2)$$

where  $r$  is the average interconnection radius (m);  $\eta$ , the gas viscosity (Pa s);  $M$ , the gas molecular weight (kg mol<sup>-1</sup>);  $R$ , the ideal gas constant (J mol<sup>-1</sup> K<sup>-1</sup>);  $T$ , the temperature (K);  $S$ , the slope of the fitted line of permeability versus pressure (mol m<sup>-2</sup> s<sup>-1</sup> Pa<sup>-2</sup>) and  $K$ , the permeability for a null pressure (mol m<sup>-2</sup> s<sup>-1</sup> Pa<sup>-1</sup>).

A pore aperture of 2.7  $\mu\text{m}$  was calculated from Eq. (2) which is in good agreement with results obtained by mercury porosimetry (Autopore 9215, Micromeritics), i.e. 1.9  $\mu\text{m}$  for an open porosity of 28 vol%.

The supports do not present deficient mechanical properties thanks to the great density of the bulk that surrounds the pores, whereas their gas permeability of  $2.88 \times 10^{-6}$  mol m<sup>-2</sup> s<sup>-1</sup> Pa<sup>-1</sup> at room temperature for an upstream pressure of 0.1 MPa is sufficient to ensure satisfactory gas diffusivity through a 1.2-mm thick support.

### 3.3. Asymmetric membrane

Asymmetric membrane fabrication can become problematic when the sintering behavior of the dense and of the support layers are dissimilar. Then, shrinkage or thermal expansion differences result in stresses or cracks in the mem-

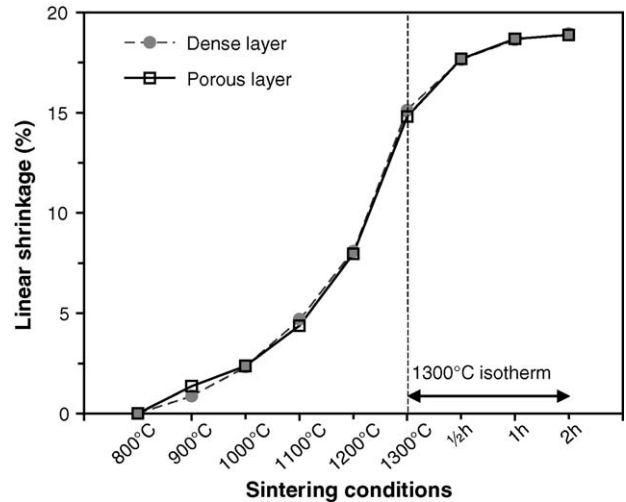


Fig. 6. Linear shrinkage of a porous and of a dense LSFG membrane vs. sintering conditions.

brane, especially when the dense layer is deposited on a pre-sintered support. So the co-sintering of these two layers is better than a double-step sintering even if it requires similar shrinkage and thermal expansion coefficients of the two materials.

Shrinkage behavior during sintering at 1300 °C with a dwell of 2 h of a dense membrane and of a fugitive particle containing membrane, measured by dilatometry (402ED, Netzsch), are identical (Fig. 6). As expected, the presence of large stable pores (8–20  $\mu\text{m}$ ) in the porous layer did not change the sintering behavior of LSFG material, and so, the co-sintering of the two materials could be performed.

Flat and crack-free co-sintered asymmetric membranes presenting a 19% diametral shrinkage were obtained (Fig. 7). Porous layer and dense layer thicknesses are respectively about 820 and 120  $\mu\text{m}$ . No delamination or interfacial reaction can be observed.

### 3.4. Catalyst coating

The LSCF catalyst has to develop the exchange surface of the membrane on a thin layer (5–30  $\mu\text{m}$ ) in order to yield a small gas flow resistance. Disk coating, with an amount of 10.3 mg cm<sup>-2</sup> of LSCF per surface area and a thermal treatment at 1000 °C for 1 h, led to a micro-porous thin layer with a homogeneous thickness of about 20  $\mu\text{m}$  (Fig. 8). A good adhesion was observed between the LSCF layer and the dense layer even if the micrograph on Fig. 8 shows a minor crack at the interface caused by the fracture of the sample. The porosity of the catalyst layer was estimated to be about 25% from its weight and thickness (calculated with a LSCF density of 6.8) and its specific surface was almost 2 m<sup>2</sup> g<sup>-1</sup> (measured on scraped catalyst fragments after thermal treatment, BET ASAP-2010, Micromeritics). These values make it possible to estimate the gas/solid interface to be about 200 cm<sup>2</sup> of catalyst per cm<sup>2</sup> of coated disk membrane.

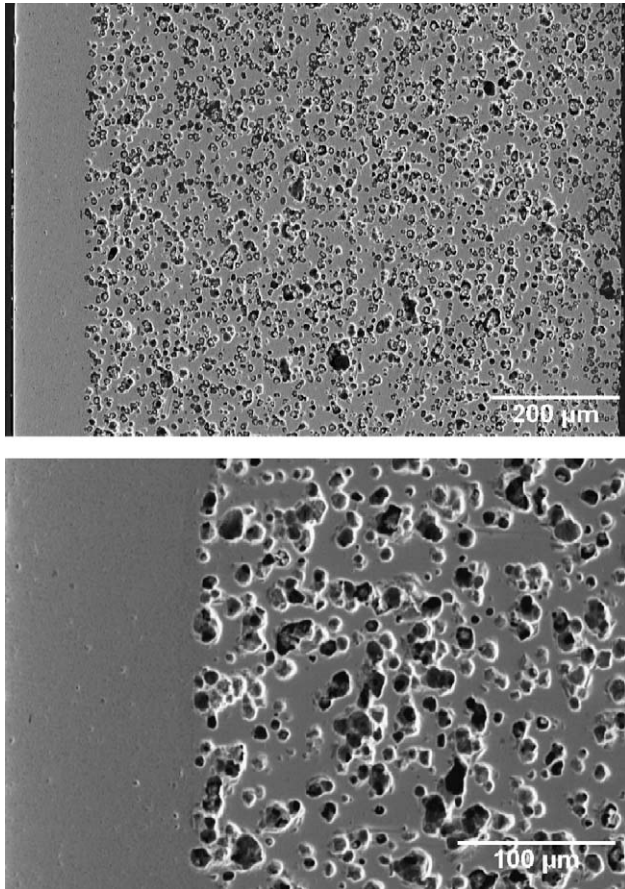


Fig. 7. SEM micrographs of a polished cross-section of an LSFG asymmetric membrane at two magnifications.

### 3.5. Oxygen permeation fluxes

Oxygen permeation fluxes measurements were performed on the membranes between 800 °C and 925 °C in an oxygen pressure gradient ( $2.1 \times 10^{-2}$  MPa on the oxygen-rich side,  $4 \times 10^{-5}$  to  $6 \times 10^{-4}$  MPa on the oxygen-lean side depending on permeation fluxes). As the overall oxygen transfer through the membrane depends on thermally activated reactions, it is common to represent the Arrhenius plots of the oxygen permeation fluxes, i.e.  $\log j_{O_2}$  versus  $1/T$ . Thus, a linear fit of the experimental data makes it possible to calculate the flux activation energy.

According to Wagner theory, the one dimensional oxygen permeation flux through a membrane placed under a chemical potential gradient can be expressed as:

$$j_{O_2} = \frac{RT}{16F^2L} \int_{\ln pO_2''}^{\ln pO_2'} \frac{\sigma_i \sigma_e}{\sigma_i + \sigma_e} d \ln(pO_2) \quad (3)$$

where  $\sigma_i$  and  $\sigma_e$  are respectively the ionic and electronic conductivity;  $F$ , the Faraday constant;  $L$ , the membrane thickness and  $pO_2'$  and  $pO_2''$  are the oxygen rich-side and oxygen lean-side partial pressure, respectively. However, this rela-

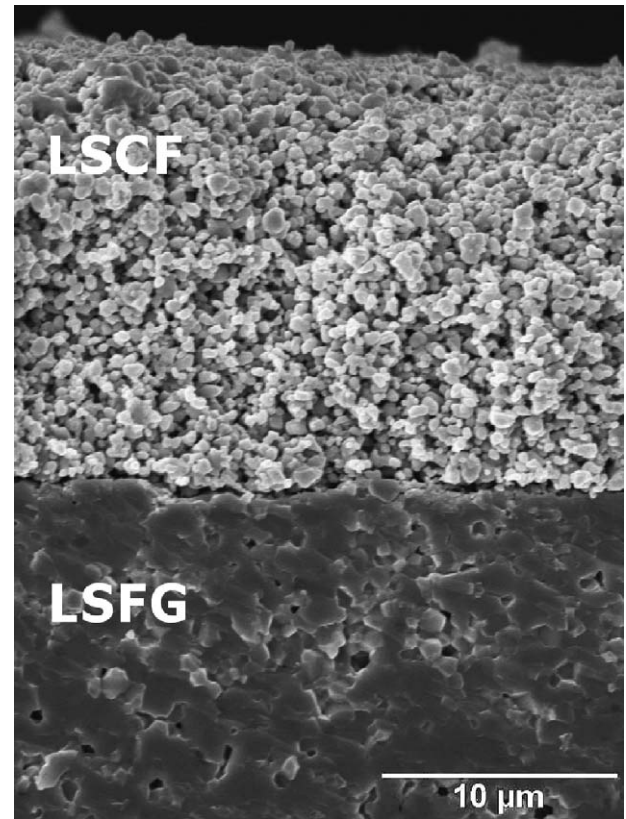


Fig. 8. Cross section of a fractured membrane: porous LSCF layer coating on a dense LSFG layer.

tion is only valid when the flux is governed by bulk oxygen diffusion which is generally true for thick membranes. But if the membrane thickness decreases below a critical value ( $L < L_c$ ), oxygen exchanges at the solid-gas interfaces become rate limiting.<sup>25</sup>

Dense LSFG membranes were tested with different thicknesses varying from 0.63 to 1.30 mm. Oxygen permeation fluxes were found to be mostly independent of membrane thickness in the range tested (Fig. 9a), while thickness normalized oxygen fluxes (by definition  $j_{O_2} \times L$ ) are clearly dependant on the membrane thickness (Fig. 9b) which is in contradiction with the Eq. (3). These results suggest that the flux through these LSFG membranes is mostly governed by oxygen surface exchanges, mechanisms previously described in the literature,<sup>37</sup> and that the critical thickness is larger than 1.30 mm. The limitation of the flux due to surface-exchange reactions in  $La_{0.5}Sr_{0.5}Fe_{0.8}Ga_{0.2}O_{3-\delta}$  was reported by Kim et al.<sup>17</sup> They estimated that the surface-exchange coefficients  $k$  of Ga-containing materials are one order of magnitude lower than that for Co-containing mixed-conducting materials or the  $La_{0.6}Sr_{0.4}FeO_{3-\delta}$  composition. However, even if the Ga-containing materials' surface-exchange coefficient is small, its oxygen permeation flux can be largely improved by using a catalyst.<sup>30</sup> In this respect, surface modification of LSFG by coating it with LSCF catalyst was expected to improve the flux and to decrease the critical thickness.

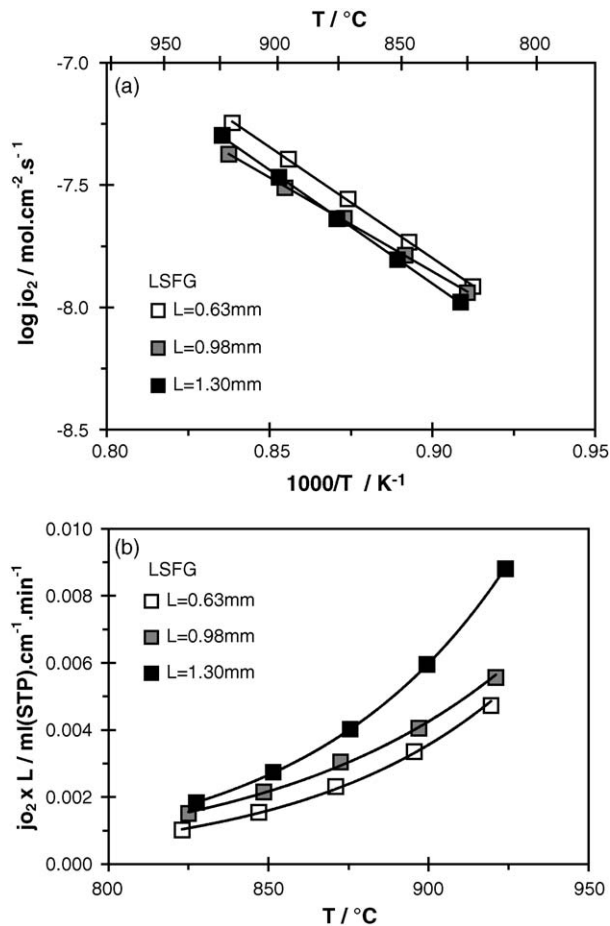


Fig. 9. Oxygen permeability of LSFG for three membrane thicknesses: (a) Arrhenius plot; (b) thickness normalized flux ( $j_{O_2} \times L$ ).

Coating both faces of 1-mm thick LSFG membranes with a LSCF porous layer made it possible to increase the oxygen flux by a factor varying between 2 and 4.5 depending on temperature (Fig. 10). At 850 °C, the oxygen flux increased from 0.022 ml cm<sup>-2</sup> min<sup>-1</sup> for LSFG to 0.084 ml cm<sup>-2</sup> min<sup>-1</sup> for fpsc-LSFG. The apparent activation energy decreased from 144 kJ mol<sup>-1</sup> for LSFG to 63 kJ mol<sup>-1</sup> for fpsc-LSFG. As expected, the LSCF catalyst porous layer appears to have a great influence on the oxygen surface exchanges. On the other hand, LSFG and psc-LSFG membranes presented the same fluxes whatever the temperature (Fig. 10) and similar apparent activation energy, i.e. 144 and 139 kJ mol<sup>-1</sup> respectively. The catalyst coating of the oxygen lean-side exposed surface is insufficient to ensure the flux improvement. The surface reaction on the oxygen-feed side of LSFG, which can be described with the overall reaction:



has a lower reaction rate than bulk diffusion and surface reaction on the permeate side. As a result, the coating of the feed-side surface by a catalyst makes it possible to increase the flux which is now governed either by bulk diffusion or by feed-side exchange or by these two mechanisms.

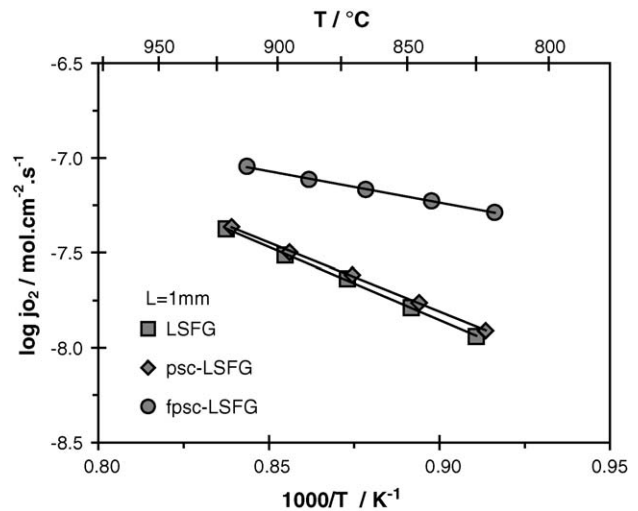


Fig. 10. Arrhenius plots of oxygen permeation fluxes of 1-mm thick LSFG membrane uncoated (LSFG), coated with LSCF on the oxygen permeate side (psc-LSFG) and coated with LSCF on both sides (fpsc-LSFG).

In order to confirm the flux limiting mechanism, asymmetric membranes were tested, with a dense layer thickness of 120 μm (Fig. 11). The dense layer was exposed to air flow and the porous one to argon flow. Oxygen fluxes through LSFG-am are similar to the ones of LSFG (Fig. 9) that confirms the weak impact of the thickness for uncoated membranes. As far as coated membranes are concerned, the oxygen permeation fluxes of LSFG asymmetric membrane coated on the dense feed side (fsc-LSFG-am) were found to be close to the ones of LSFG thick membrane coated on both sides (fpsc-LSFG) (Fig. 10). The apparent activation energy of fsc-LSFG-am was found to be 79 kJ mol<sup>-1</sup>. As the dense layer thickness of the asymmetric membrane (120 μm) is much lower than the

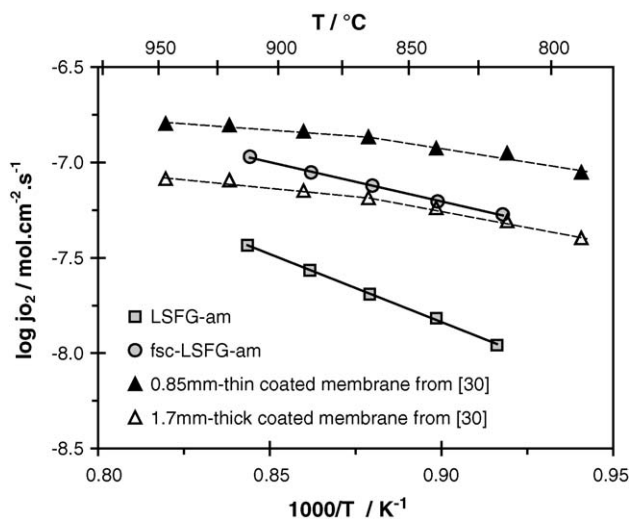


Fig. 11. Arrhenius plots of oxygen permeation fluxes of asymmetric membranes, uncoated (LSFG-am) and coated on the air side (fsc-LSFG-am). Comparison with literature data<sup>30</sup> with  $L=0.85\text{ mm}$  (thin membrane) and  $L=1.7\text{ mm}$  (thick membrane).



one of fpsc-LSFG (1 mm), the membrane thickness does not seem to play a critical role for the membrane performance even if a catalyst was used on its oxygen feed-side. These results confirm that the oxygen exchange on the oxygen rich-side exposed surface is the rate determining step both for uncoated and coated membranes.

This behavior is different from the study reported by Lee et al.<sup>30</sup> They found that the thickness of a  $\text{La}_{0.7}\text{Sr}_{0.3}\text{Fe}_{0.4}\text{Ga}_{0.6}\text{O}_{3-\delta}$  membrane coated with  $\text{La}_{0.6}\text{Sr}_{0.4}\text{CoO}_{3-\delta}$  on both surfaces had an influence on the flux in good agreement with Wagner's theory. Their results are compared on Fig. 11 for two thicknesses, i.e. for a 0.85-mm thin membrane and a 1.7-mm thick membrane. The values of the fluxes and of the activation energies are similar for our system and Lee's one. However, with the assumption that the Wagner's law was still verified in Lee's system until a thickness of 120  $\mu\text{m}$ , a 120- $\mu\text{m}$  thick membrane should present a flux as  $\log j_{\text{O}_2} = -6.0 \text{ mol cm}^{-2} \text{ s}^{-1}$  at 890 °C, and so an order of magnitude larger than the one we measured. The difference in thickness dependence is supposed to be caused by the catalyst nature or morphology. In other words, catalytic activity of  $\text{La}_{0.6}\text{Sr}_{0.4}\text{CoO}_{3-\delta}$  used by Lee could be better than  $\text{La}_{0.6}\text{Sr}_{0.4}\text{Fe}_{0.8}\text{Ga}_{0.2}\text{O}_{3-\delta}$  but the differences in grain size and distribution on the surface may also be important. In addition, Lee et al. observed an intermediate layer derived from the reaction between membrane and catalyst materials of composition  $(\text{La}_{1-x}\text{Sr}_x)(\text{Co}_y\text{Ga}_y\text{Fe}_{1-y-y'})\text{O}_{3-\delta}$  that wasn't detected in our membranes and that can have an effect on near-surface bulk properties.

To summarize, our coated-membrane performances are in good agreement with literature data but oxygen permeation rate is strongly dependant on oxygen surface-exchange. To improve oxygen fluxes, a study of the surface catalyst has to be made to determine the influence of its composition and microstructure on oxygen reduction and re-oxidation kinetics.

#### 4. Conclusions

The synthesis of the perovskite compositions  $\text{La}_{0.6}\text{Sr}_{0.4}\text{Fe}_{0.9}\text{Ga}_{0.1}\text{O}_{3-\delta}$  (LSFG) and  $\text{La}_{0.6}\text{Sr}_{0.4}\text{Co}_{0.8}\text{Fe}_{0.2}\text{O}_{3-\delta}$  (LSCF) was achieved using a solid-state reaction route. LSFG powder was successfully shaped into self-supported and asymmetric membranes via a tape-casting and lamination process. Crack-free and flat asymmetric membranes were obtained after sintering when the porosity of the support layer was formed by large corn-starch particles as pore forming agent. The shrinkages of the dense and of the porous layers were identical and the final porosity in the support was mostly governed by the amount and size of the fugitive particles that were incorporated.

Porous coating of LSCF on the membrane surface without delamination was performed using screen-printing. After thermal treatment, the surface area developed by a 20- $\mu\text{m}$  thick catalytic layer was found to be about 200  $\text{cm}^2$  per  $\text{cm}^2$

of membrane area. LSFG and LSCF materials did not present any interfacial reactions.

The thickness of uncoated LSFG-membrane was found to have small or negligible effect on oxygen permeation fluxes (0.022  $\text{ml cm}^{-2} \text{ min}^{-1}$  at 850 °C) that indicates a surface exchange driven mode in our experimental conditions. On the other hand, coated membranes present a significant enhancement of the fluxes (0.084  $\text{ml cm}^{-2} \text{ min}^{-1}$  at 850 °C for a permeate and feed-side coating 1 mm thick membrane). Based on these experiments, it has been determined that the oxygen transport is mainly limited by surface reactions on the air exposed face of the membrane.

Similar results were obtained on a coated asymmetric membrane since decreasing the thickness did not bring flux improvement. Even if the LSCF coating of LSFG membrane on its oxygen feed side has a positive effect on the flux, the surface reactions seem to remain limiting for the overall permeation rate. The catalytic layer nature and its microstructure have to be studied to improve the overall oxygen permeation fluxes.

#### Acknowledgements

The authors want to express their gratitude to *Air Liquide* and *CNRS* for supporting this research.

#### References

1. Rostrup-Nielsen, J. R., Catalysis and large-scale conversion of natural gas. *Catal. Today*, 1994, **21**, 257–267.
2. Sammells, A. F., Schwartz, M., Mackay, R. A., Barton, T. F. and Peterson, D. R., Catalytic membrane reactors for spontaneous synthesis gas production. *Catal. Today*, 2000, **56**, 325–328.
3. Wilhelm, D. J., Simbeck, D. R., Karp, A. D. and Dickenson, R. L., Syngas production for gas-to-liquids applications: technologies, issues and outlook. *Fuel Process. Technol.*, 2001, **71**, 139–148.
4. Armor, J. N., Applications of catalytic inorganic membrane reactors to refinery products. *J. Membr. Sci.*, 1998, **147**, 217–233.
5. Balachandran, U., Dusek, J. T., Mieville, R. L., Poeppel, R. B., Kleefisch, M. S., Pei, S. *et al.*, Dense ceramic membranes for partial oxidation of methane to syngas. *Appl. Catal. A: Gen.*, 1995, **133**, 19–29.
6. Hazbun, E. A., Ceramic membrane and use thereof for hydrocarbon conversion, US Patent 4,827,071 (2 May 1989).
7. Thorogood, R. M., Srinivasan, R., Yee T. F. and Drake, M. P., Composite mixed conductor membranes for producing oxygen, US Patent 5,240,480 (31 August 1993).
8. Gottzmann, C. F., Prasad, R. and Schwartz, J. M., Syngas reactor with ceramic membrane, Eur. Patent 0,962,422,B1 (1999).
9. Schwartz, M., White, J. H. and Sammells, A. F., Solid state oxygen anion and electron mediating membrane and catalytic membrane reactors containing them, US Patent 6,033,632 (7 March 2000).
10. Mazanec, T. J. and Cable, T. L., Oxygen permeable mixed conductor membranes, US Patent 5,648,304 (15 July 1997).
11. Tsai, C. Y., Dixon, A. G., Moser, W. R. and Ma, Y. H., Dense perovskite membrane reactors for partial oxidation of methane to syngas. *AIChE J.*, 1997, **43**(11), 2741–2750.
12. Teraoka, Y., Zhang, H. M., Okamoto, K. and Yamazoe, N., Mixed ionic-electronic conductivity of  $\text{La}_{1-x}\text{Sr}_x\text{Co}_{1-y}\text{Fe}_y\text{O}_{3-\delta}$  perovskite-type oxides. *Mater. Res. Bull.*, 1988, **23**, 51–58.



13. Teraoka, Y., Zhang, H. M., Furukawa, S. and Yamazoe, N., Oxygen permeation through perovskite-type oxides. *Chem. Lett.*, 1985, 1743–1746.
14. Gellings, P. J. and Bouwmeester, H. J. M., Ion and mixed conducting oxides as catalysts. *Catal. Today*, 1992, **12**, 1–105.
15. Kharton, V. V., Yaremchenko, A. A., Kovalevsky, A. V., Viskup, A. P., Naumovich, E. N. and Kerko, P. F., Perovskite-type oxides for high-temperature oxygen separation membranes. *J. Membr. Sci.*, 1999, **163**, 307–317.
16. Bouwmeester, H. J. M., Dense ceramic membranes for methane conversion. *Catal. Today*, 2003, **82**, 141–150.
17. Kim, S., Wang, S., Chen, X., Yang, Y. L., Wu, N., Ignatiev, A. et al., Oxygen surface exchange in mixed ionic electronic conductors: application to  $\text{La}_{0.5}\text{Sr}_{0.5}\text{Fe}_{0.8}\text{Ga}_{0.2}\text{O}_{3-d}$ . *J. Electrochem. Soc.*, 2000, **147**(6), 2398–2406.
18. Ishihara, T., Yamada, T., Arikawa, H., Nishiguchi, H. and Takita, Y., Mixed electronic-oxide ionic conductivity and oxygen permeating property of Fe-, Co- or Ni-doped  $\text{LaGaO}_3$  perovskite oxide. *Solid State Ionics*, 2000, **135**, 631–636.
19. Ishihara, T., Tsuruta, Y., Todaka, T., Nishiguchi, H. and Takita, Y., Fe doped  $\text{LaGaO}_3$  perovskite oxide as an oxygen separating membrane for  $\text{CH}_4$  partial oxidation. *Solid State Ionics*, 2002, **152**, 709–714.
20. Kharton, V. V., Shaulo, A. L., Viskup, A. P., Avdeev, M., Yaremchenko, A. A., Patrakeevev, M. V. et al., Perovskite-like system  $(\text{Sr},\text{La})(\text{Fe},\text{Ga})\text{O}_{3-\delta}$ : structure and ionic transport under oxidizing conditions. *Solid State Ionics*, 2002, **150**, 229–243.
21. Kharton, V. V., Yaremchenko, A. A., Patrakeevev, M. V., Naumovich, E. N. and Marques, F. M. B., Thermal and chemical induced expansion of  $\text{La}_{0.3}\text{Sr}_{0.7}(\text{Fe},\text{Ga})\text{O}_{3-\delta}$ . *J. Eur. Ceram. Soc.*, 2003, **23**, 1417–1426.
22. Ritchie, J. T., Richardson, J. T. and Dan, L., Ceramic membrane reactor for synthesis gas production. *AIChE J.*, 2001, **47**(9), 2092–2101.
23. Bredesen, R., Sogge, J., In Paper Presented at The United Nations Economic Commission for Europe Seminar on Ecological Applications of Innovative Membrane Technology in Chemical Industry, Chem/Sem. 21/R.12, Cetaro, Calabria, Italy, 1–4 May 1996.
24. Teraoka, Y., Fukuda, T., Miura, N. and Yamazoe, N., Development of oxygen semipermeable membrane using mixed conductive perovskite-type oxides (part 2). *J. Ceram. Soc. Jpn. Int. Ed.*, 1989, **97**, 523.
25. Chen, C. H., Bouwmeester, H. J. M., Van Doorn, R. H. E., Kruidhof, H. and Burggraaf, A. J., Oxygen permeation of  $\text{La}_{0.3}\text{Sr}_{0.7}\text{CoO}_{3-\delta}$ . *Solid State Ionics*, 1997, **98**, 7–13.
26. Jin, W., Li, S., Huang, P., Xu, N. and Shi, J., Preparation of an asymmetric perovskite-type membrane and its oxygen permeability. *J. Membr. Sci.*, 2001, **185**, 237–243.
27. Hong, L., Chen, X. and Cao, Z., Preparation of a perovskite  $\text{La}_{0.2}\text{Sr}_{0.8}\text{CoO}_{3-x}$  membrane on a porous MgO substrate. *J. Eur. Ceram. Soc.*, 2001, **21**, 2207–2215.
28. Middleton, H., Diethelm, S., Ihringer, R., Larrain, D., Sfeir, J. and Van Herle, J., Co-casting and co-sintering of porous MgO support plates with thin dense perovskite layers of  $\text{LaSrFeCoO}_3$ . *J. Eur. Ceram. Soc.*, 2004, **24**, 1083–1086.
29. Lee, K. S., Lee, S., Kim, J. W. and Woo, S. K., Enhancement of oxygen permeation by  $\text{La}_{0.6}\text{Sr}_{0.4}\text{CoO}_{3-\delta}$  coating in  $\text{La}_{0.7}\text{Sr}_{0.3}\text{Ga}_{0.6}\text{Fe}_{0.4}\text{O}_{3-\delta}$ . *Desalination*, 2002, **147**, 439–444.
30. Lee, S., Lee, K. S., Woo, S. K., Kim, J. W., Ishihara, T. and Kim, D. K., Oxygen-permeating property of  $\text{LaSrBFeO}_3$  (B=Co, Ga) perovskite membrane surface-modified by  $\text{LaSrCoO}_3$ . *Solid State Ionics*, 2003, **158**, 287–296.
31. Kharton, V. V., Kovalevsky, A. V., Yaremchenko, A. A., Figueiredo, F. M., Naumovich, E. N., Shaulo, A. L. et al., Surface modification of  $\text{La}_{0.3}\text{Sr}_{0.7}\text{CoO}_{3-\delta}$  ceramic membranes. *J. Membr. Sci.*, 2002, **195**, 277–287.
32. Teraoka, Y., Honbe, Y., Ishii, J., Furukawa, H. and Moriguchi, I., Catalytic effects in oxygen permeation through mixed-conductive LSCF perovskite membranes. *Solid State Ionics*, 2002, **152-153**, 681–687.
33. Tsiakaras, P., Marnellos, G., Athanasiou, C., Stoukides, M., ten Elshof, J. E., Bouwmeester, H. J. M. et al., Electrode polarization and electrical properties of the  $\text{La}_{0.6}\text{Sr}_{0.4}\text{Co}_{0.8}\text{Fe}_{0.2}\text{O}_{3-\delta}$ .  $\text{O}_2/\text{yttria}$  stabilized zirconia interface: Effect of gas phase composition and temperature. *Solid State Ionics*, 1996, **86**, 1451–1456.
34. Etchegoyen, G., Chartier, T., Julian, A. and Del-Gallo, P., Microstructure and oxygen permeability of a  $\text{La}_{0.6}\text{Sr}_{0.4}\text{Fe}_{0.9}\text{Ga}_{0.1}\text{O}_{3-\delta}$  membrane containing magnesia as dispersed second phase particles, *J. Membr. Sci.*, in press.
35. Benito, J. M., Conesa, A., Rubio, F. and Rodriguez, M. A., Preparation and characterization of tubular ceramic membranes for treatment of oil emulsions. *J. Eur. Ceram. Soc.*, 2005, **25**, 1895–1903.
36. Qi, X., Akin, F. T. and Lin, Y. S., Ceramic-glass composite high temperature seals for dense ionic-conducting ceramic membranes. *J. Membr. Sci.*, 2001, **193**, 185–193.
37. Ishihara, T., Kilner, J. A., Honda, M., Sakai, N., Yokokawa, H. and Takita, Y., Oxygen surface exchange and diffusion in  $\text{LaGaO}_3$  based perovskite type oxides. *Solid State Ionics*, 1998, **113**, 593–600.